Determination of pressure data from velocity data with a view towards its application in cardiovascular mechanics. Part 2: a study of aortic valve stenosis.

H. Švihlová[a,*], J. Hron[a], J. Málek[a], K. R. Rajagopal[b], K. Rajagopal[c]

[a]*Charles University in Prague, Faculty of Mathematics and Physics, Mathematical Institute, Sokolovská 83, 186 75 Prague, Czech Republic*
[b]*Texas A&M University, Department of Mechanical Engineering, College Station, TX 77843-3132, United States*
[c]*University of Texas-Houston/Memorial Hermann Texas Medical Center, Center for Advanced Heart Failure, 6411 Fannin, Houston, TX 77030, United States*

Abstract

This paper is Part 2 of a study of blood flow across cardiovascular stenoses. In Part 1, we developed a rigorous mathematical approach for deriving a pressure field from experimental data for a velocity field that can be obtained by direct measurement. In this Part, existing methods for quantifying stenoses, with specific reference to cardiac valves, are reviewed. Using the mathematically rigorous and physically accurate approach that we developed in Part 1, for a pre-specified flow velocity field proximal to the stenosis and pressure waveform field distal to the stenosis, we ascertain the intro-stenosis and distal flow velocity field, pressure field proximal and within the stenosis, and energy dissipation, all as function of position and time. The computed dissipation, kinetic energy and pressure are then presented in an idealized geometry, but with realistic geometry, with a symmetric stenosis.

Keywords: Dissipation, Heart Valve, Stenosis, Navier-Stokes Equation, Blood Vessel.

1. Introduction

Stenotic cardiac valve and arterial occlusive diseases are among the leading causes of death worldwide; see Go et al. (2013). Interventional and surgical treatments have provided improvements in survival, cardiac function, and functional capacity. However, procedural therapies have substantial risks, and benefits are proportional to the physiological severity of the stenoses treated. Consequently, accurate and precise assessment of stenosis severity is required in order to appropriately decide whether and what type of treatment is warranted for a given lesion.

A stenosis in the cardiovascular system is a reduction in cross-sectional area of a structure across which blood flows. An anatomic stenosis, which is simply defined by its existence, may or may not result in a physiologically important stenosis. The physiological impact of a stenosis is the extent to which it poses increased impedance to blood flow, i.e., the extent to which energy of the flowing blood is dissipated or lost in order to generate and maintain flow and ultimately, to which blood flow becomes impaired. Stenoses are generally treated when they are physiologically important. Physiologically important stenoses satisfy two criteria: (1) hemodynamic severity, and more importantly, (2) adverse effects on proximal (e.g., the left ventricle in aortic valve stenosis) or distal (e.g., myocardial territory in the distribution of a stenotic coronary artery) tissues and organs.

Both invasive and non-invasive diagnostic techniques have been used to assess cardiovascular stenoses; see Bhattacharyya et al. (2013); Leggett and Otto (1996); Carroll (1993). While invasive techniques accurately determine hemodynamic severity and are the historical gold standard, they carry procedural risks.

---

*Corresponding author
Email addresses: helena.svihlova@seznam.cz (H. Švihlová), jaroslav.hron@mff.cuni.cz (J. Hron), josef.malek@mff.cuni.cz (J. Málek), krajagopal@tamu.edu (K. R. Rajagopal), keshava.rajagopal@gmail.com (K. Rajagopal)

Consequently, non-invasive techniques have been used increasingly. However, as we outline below, current approaches to interpreting non-invasive data are incapable of ascertaining physiologic stenosis severity. In this manuscript, we develop an improved approach to determination of the energy dissipation in the flowing blood and pressure gradients and differences across cardiovascular stenoses, which can be applied to non-invasive diagnostic modalities.

Background

Various methods have been used to evaluate stenoses by either anatomic or physiologic criteria. Broadly, anatomic approaches either directly measure cross-sectional area, or invoke conservation of mass to calculate cross-sectional area. In contrast, physiological approaches directly measure intraluminal pressure and/or flow velocity. Measured trans-stenosis pressure difference and calculated stenosis "resistance" or "impedance" are conceptually sound assessments of the physiologic impact of a stenosis. However, other physiological approaches used currently, notably calculated intraluminal pressure derived from measured flow velocity, or even calculated cross-sectional area derived from measured intraluminal pressure and volumetric flow rate, are fundamentally unsound from a fluid mechanical perspective. The relative strengths and weaknesses of these various approaches are reviewed below. Figures 1 - 3 depict the left-sided cardiac valves (aortic and mitral) and the physiology of cardiovascular stenoses.

1.1. Anatomic

Direct measurement of valve or arterial cross-sectional area historically has been both inaccurate and imprecise. However, conservation of mass is applicable over one or more cardiac cycles because the circulation is a closed system and blood is an incompressible material, even with deformable conduits. Thus, the mean volumetric flow rate is constant along a given conduit, assuming the absence of branch vessels. The cross-sectional area at a given location along the length of the conduit thus may be calculated, as it equals the mean volumetric flow rate over a cardiac cycle divided by the magnitude of the mean flow velocity through the cross-sectional area in question over a cardiac cycle; see Warth et al. (1984); Kosturakis et al. (1984). Cardiac valve area and arterial (carotid) cross-sectional area have been determined using this "continuity"-based approach; see Rodriguez et al. (2011); Alexandrov et al. (1993). However, utilization of conservation of mass-based approaches only permits determination of cross-sectional area, i.e., whether an anatomic stenosis is present, not whether it is physiologically important.

1.2. Physiologic

A range of strategies have been developed to determine the physiological significance of a stenosis. These are listed and discussed below. While 1.2.1, 1.2.2, 1.2.3 are invasive methods, 1.2.4 is a non-invasive.

1.2.1. Trans-stenosis pressure difference ("pressure gradient")

In a conduit with the same cross-sectional area proximal and distal to the stenosis, the magnitude of the mean flow velocity (over a cardiac cycle) is the same at the proximal and distal locations, and consequently the kinetic energy of the flowing blood is unchanged. In the absence of changes in gravitational potential energy, the mean pressure decreases across the stenosis, thus is equal to amount of energy dissipated across the stenosis as

$$Edis = |p_{prox} - p_{dist}|_{mean}. \tag{1}$$

The absolute value of the trans-stenosis mean pressure difference thus reflects the physiological impact of the stenosis. However, it is also proportional to the mean volumetric flow rate (and the proximal pressure and total energy of the flowing blood), and consequently, the absolute trans-stenosis pressure difference is not a parameter that is solely determined by the properties of the stenosis.

1.2.2. Resistance and impedance

A physiologically relevant stenosis is defined by the extent to which it impedes blood flow. Consequently, the usage of resistance to quantify stenosis severity is relatively sound from a conceptual standpoint; see Ford et al. (1990); Eckstein et al. (1946). Resistance is defined as the mean pressure difference across the stenosis divided by the mean flow rate, thus

$$R = \frac{|p_{prox} - p_{dist}|_{mean}}{Q_{mean}} \tag{2}$$

However, in reality proximal and distal pressures, and volumetric flow rate, vary differentially as functions of time; consequently, resistance may vary as a function of time. The mechanical basis for this is complex, and is largely due to the non-linear mechanical properties of both the ventricular myocardium that intermittently generates arterial blood flow, as well as the non-linear deformability of cardiovascular conduits. This is particularly true for cardiac valves, the orifices of which may change substantially during the period of trans-valvular flow (systolic ejection for the aortic and pulmonary valves, diastolic filling for the mitral and tricuspid valves). Thus, the notion of "impedance" – which incorporates the time-varying characteristics of pressure and flow profiles in quantifying mechanical properties of cardiovascular conduits - has been similarly co-opted from circuit theory and applied to both cardiac valves and the arterial circulation; see (Schwartz et al., 1997, 1991; Attinger et al., 1966; Spencer and Edmunds, 1968). While both resistance and impedance are truly intrinsic material parameters – although modifiable by hemodynamic forces, rigorous determination of either one requires measurement of proximal and distal pressures – necessitating invasiveness, along with volumetric flow rate.

1.2.3. Valve area (Gorlin/Hakki Gorlin and Gorlin (1951))

While valve area is strictly an anatomical assessment of stenosis severity for cardiac valves, physiological approaches have been employed to ascertain valve area. The archetype for this approach was developed by Gorlin and Gorlin; see Gorlin and Gorlin (1951), with subsequent simplifications by Hakki et al.; see Hakki et al. (1981). Using rudimentary hydraulics, Gorlin determined that valve area is equal to the mean volumetric flow rate divided by the product of the square root of the mean transvalvular pressure difference and an empirical constant.

$$A_{valve} = \frac{Q_{mean}}{C\sqrt{|p_{prox} - p_{dist}|_{mean}}} \tag{3}$$

However, the mechanical basis for the Gorlin equation rests on Torricelli's empirical modification of the Bernoulli equation, i.e., the "constant" used is actually variable, and its value is in fact what describes energy dissipation. Moreover, as discussed below, the Bernoulli equation itself is an expression of conservation of energy, and thus is incapable of quantifying energy dissipation. Modifications of the Bernoulli equation using additional energy dissipation factors such as those in the Gorlin equation are totally empirical and in fact variable from condition to condition – without a basis in mechanics or mathematics that is reproducible across experimental conditions. Consequently, such approaches lack accurate and precise predictive capacity requisite of any sound theoretical model.

### 1.2.4. Derived trans-stenosis pressure difference

Non-invasive techniques have been used to calculate trans-stenosis pressure differences, as opposed to invasive direct measurements. In clinical parlance these differences are termed "pressure gradients," which is inaccurate. This approach also utilizes the Bernoulli equation. However, it is unlike the Gorlin-type approach specifically applied to heart valves, which at least incorporates an empirical constant to attempt to express energy dissipation (which in reality is actually highly variable). Rather, the Bernoulli equation is manipulated to allow determination of energy dissipation, even though it is an expression of energy conservation. It is conveniently assumed that energy losses in the flowing blood all occur at the outlet of a stenosis. As a consequence, the energy losses in the flowing blood can be expressed exclusively as losses in kinetic energy, and the pressure within the stenosis is equal to the pressure downstream of the stenosis. Further, the pressure difference across the stenosis is thus equal to the loss in kinetic energy, which can be easily

calculated based on non-invasively measured flow velocities at different locations relative to the stenosis. This approach has no rational basis, but loose correlations between non-invasively derived and invasively measured "pressure gradients" have been demonstrated. Moreover, other studies have demonstrated poor correlation between echocardiography calculations and catheterization measurements; see Fischer et al. (1995); Berger et al. (1984), where the correlation coefficient $r = 0.79$, Doppler gradient $= 0.66 \cdot$ (catheter gradient) $+ 17.3$.

The characteristic approach; see Hatle et al. (1978, 1980) is to make a modification to Bernoulli's equation by introducing an *ad hoc* term that purportedly accounts for the dissipation; see Akins et al. (2008), see Dasi et al. (2009). First, Bernoulli's equation applies to flows of ideal fluids while blood is a viscous fluid. Thus, such an approach is completely unwarranted. Second, the pressure-velocity pair $(p_E, \mathbf{v}_E)$ that solves the flow of an ideal Euler fluid that appears in Bernoulli's equation is far different from the pressure-velocity pair $(p_{NS}, \mathbf{v}_{NS})$ that solves the Navier-Stokes equation. Third, the methodology adopted to estimate the *ad hoc* dissipation term that is added to Bernoulli's equation is flawed, since it double counts several of the sources for the dissipation by not recognizing that these terms are inter-related, with these contributions not added as though they were a consequence of a linear problem - wherein such effects could be superposed.

As mentioned above, a variety of mechanisms contribute to energy losses, see Akins et al. (2008): so called "viscous losses", "turbulent losses", "flow separation losses", etc. However, these losses are not independent or additive. More importantly, Bernoulli's equation is absolutely mute with regard to all three of these losses, or for that matter, any energy losses. The physical basis for all of these types of energy losses is viscosity. However, the Bernoulli equation based approach assumes an inviscid fluid. Finally, with regards to turbulence, no current model is capable of describing the relevant phenomena; we note the modeling of turbulent flows has remained one of the most important unsolved problems in mechanics. Thus, to merely appeal to an *ad hoc* modification of Bernoulli's equation incorrectly suggests that a more rigorous approach is being employed than that which is actually used. The thesis of this manuscript is that more mathematically rigorous and physically relevant approaches to studying the mechanics of blood flow across cardiovascular stenoses can be developed. In Part 1 of this study; see Švihlová et al. (2016), we discussed a rigorous new mathematical procedure for the determination of the pressure (normal stress) field, from pre-specified data for the velocity field that can be obtained through imaging procedures such as 4D Magnetic Resonance Imaging or Echocardiography.

In this paper, we focus on aortic valve stenosis as an example to apply the approach. Specifically, for a pre-specified left ventricular outflow tract velocity profile and ascending thoracic aortic pressure profile as inflow and outflow boundary conditions we determine pressure, velocity, and energy dissipation as functions of the entire spatial field (left ventricular outflow tract, aortic valve/root, and proximal ascending thoracic aorta) and time.

A

B
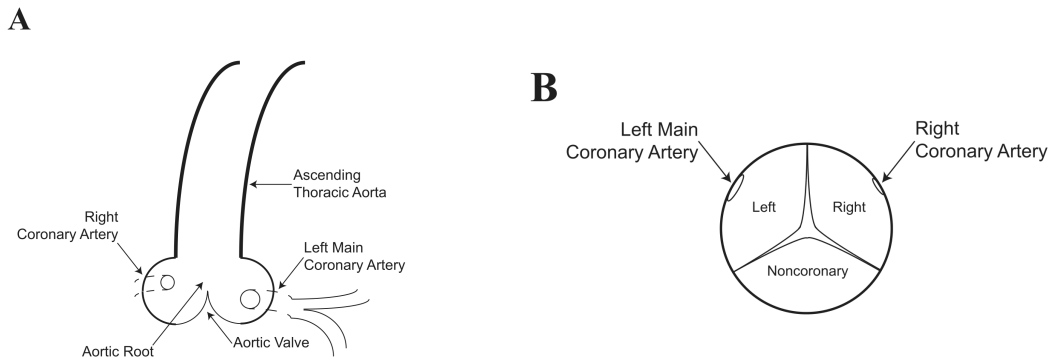
Figure 1: **Anatomy of the human aortic valve/root complex.** The aortic valve, comprised of three cusps (leaflets), is shown in the diagram as being attached to the aortic root circumferentially, forming a circumferentially thickened ridge of fused cusp/aortic tissue termed the aortic valve annulus. The annulus is a three-dimensional crown-like structure, as opposed to a planar structure. In addition, the diameter of the base of the annulus (ventriculo-aortic junction) is smaller than the diameter of the aortic root-ascending thoracic aortic junction (a.k.a. sinotubular junction), such that the annulus is within a conic section; this is not depicted to scale in **A**. The aortic root constitutes the tissue housing for the valve; the root tissues are comprised of the three sinuses of Valsalva. At the initiation of left ventricular systolic ejection, the left ventricular outflow tract-to-aortic root pressure gradient forces the cusps of the aortic valve radially outwards, increasing the orifice cross-sectional area and permitting blood flow out of the left ventricle and into the aortic root throughout systolic ejection, and thence downstream. At the end of left ventricular systolic ejection, the aortic root-to-left ventricular outflow tract pressure gradient forces the cusps radially inwards, resulting in circumferential cusp coaptation and elimination of the potential orifice for regurgitant blood flow back into the left ventricular cavity. The left sinus of Valsalva is typically slightly smaller than the two other sinuses (not shown to scale), the right and noncoronary sinuses. The left main and right coronary arteries, which provide cardiac tissue/myocardial blood flow, each arise as separate ostia from the left and right sinuses of Valsalva, respectively. The segment of aorta downstream of/distal to the aortic root is termed the ascending thoracic aorta, which does not contain branch arteries. **A.** Long-axis view. In this view, not all three cusps can be seen. Rather, cross sections of the right and left cusps are shown. The view demonstrates the valve during either systolic isovolumetric contraction, or either phase of diastole. **B.** Short-axis view. In this view, all three cusps can be visualized. This view is an approximate representation of the surgeon's view of the aortic valve/root complex when the ascending thoracic aorta has been transected proximally. The view also demonstrates the valve during systolic isovolumetric contraction, or either phase of diastole. A central orifice is merely presented to highlight the separate nature of each valve cusp; in reality, a competent (non-regurgitant) valve has a minimal or absent central orifice.

A

B
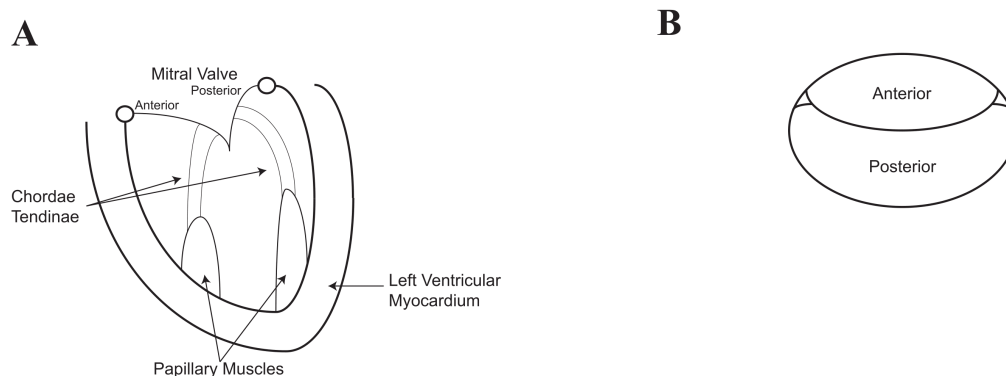
Figure 2: **Anatomy of the human mitral valve/subvalvular apparatus complex.** The mitral valve, comprised of two leaflets (anterior and posterior), is shown in the diagram as being attached to the mitral valve annulus, which is a circumferential roughly planar (actually "saddle" shaped) ring of tissue that demarcates the left atrium and the left ventricle, in contrast to the three-dimensional annulus of the aortic valve. The mitral valve leaflets insert into the annulus circumferentially, with a tiny separation present at the medial and lateral commissures (junctions of the leaflets with one another). The leaflets are attached to chordae tendinae, which anchor to the papillary muscles of the left ventricle. The coaptation surface between the two leaflets is not actually at the edges of the leaflets, but rather, from surface contacts between the two leaflet faces. At the initiation of left ventricular diastolic filling, the left atrium-to-left ventricle pressure gradient, along with relaxation of the papillary muscles to which the mitral valve leaflets attach, opens the mitral valve radially outwards, increasing the orifice cross-sectional area and permitting blood flow out of the left atrium and into the left ventricle throughout diastolic filling. At the end of left ventricular filling (following atrial contraction), the left ventricle-to-left atrium pressure gradient and papillary muscle contraction act in concert to force the mitral valve closed, resulting in circumferential leaflet coaptation and elimination of the potential orifice for regurgitant blood flow back into the left atrial cavity. The anterior leaflet of the mitral valve has a larger radial extent, but a smaller circumferential extent, than the posterior leaflet. **A.** Long-axis view. In this view, the larger radial extent of the anterior leaflet can be readily appreciated. Chordae tendinae and the left ventricular papillary muscles are depicted. The view demonstrates the valve during either phase of systole, or isovolumetric diastolic relaxation. **B.** Short-axis view. This view is an approximate representation of the surgeon's view of the mitral valve through a left atrial exposure. The view also demonstrates the valve during either phase of systole, or diastolic isovolumetric relaxation.
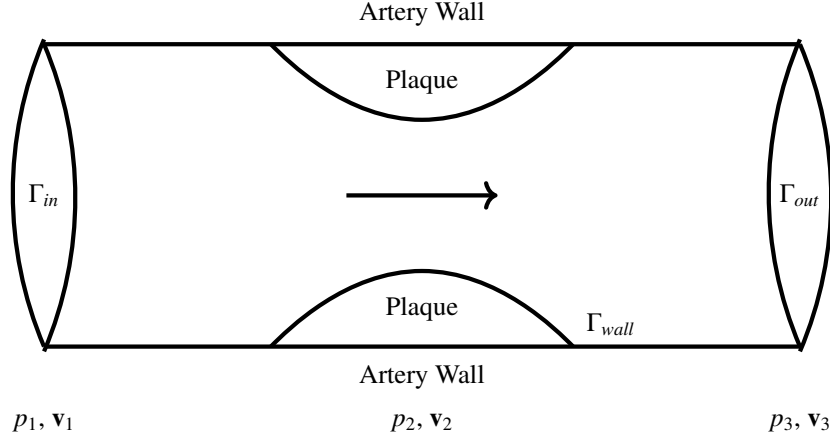
Real fluid: $p_1 > p_3 > p_2$; $|\mathbf{v}_1| = |\mathbf{v}_3| < |\mathbf{v}_2|$

Ideal fluid (Bernoulli): $p_1 = p_3 > p_2$; $|\mathbf{v}_1| = |\mathbf{v}_3| < |\mathbf{v}_2|$

Forced Application of Ideal fluid to Real fluid: $p_1 > p_3 = p_2$; $|\mathbf{v}_1| = |\mathbf{v}_3| < |\mathbf{v}_2|$

Figure 3: **Schematic of an arterial stenosis.** The diagram depicts an idealized stenosis within an artery; 1 = upstream of/proximal to the stenosis, 2 = within the stenosis, 3 = downstream of/distal to the stenosis. For an ideal fluid, conservation of energy applies, and $p_1 = p_3 > p_2$, $|\mathbf{v}_1| = |\mathbf{v}_3| < |\mathbf{v}_2|$. The degree of p_2 decrease and $|\mathbf{v}_2|$ increase is determined by conservation of energy, with conservation of mass satisfied as well. For the real case of flowing blood, $p_1 > p_3$ [with $(p_1 - p_3)$ quantifying the energy loss], typically $p_3 > p_2$ (but in principle p_3 can be $\leq p_2$), and $|\mathbf{v}_1| = |\mathbf{v}_3| < |\mathbf{v}_2|$. When the Bernoulli equation is contrived to be used in the setting of energy dissipation, it is conveniently assumed that the pressure within the stenosis is equal to the pressure downstream of/distal to the stenosis, even though this lacks a rational basis. In this setting, $p_1 > p_2 = p_3$ (that is, $p_1 > p_2$, $p_1 > p_3$, and $p_2 = p_3$), and $|\mathbf{v}_1| = |\mathbf{v}_3| < |\mathbf{v}_2|$. Thus, $p_1 - p_3$ happens to be equal to the loss in kinetic energy between the segments within the stenosis and downstream of/distal to the stenosis ($1/2\rho|\mathbf{v}_2|^2 - 1/2\rho|\mathbf{v}_3|^2$). This unfounded assumption permits calculation of the trans-stenosis pressure difference indirectly, by determining the loss in kinetic energy.

2. Determination of the energy dissipation

Let us suppose that the flow of blood can be described by the Navier-Stokes equations for an incompressible fluid, as was described at Part 1, namely

$$\text{div } \mathbf{v} = 0$$
$$\frac{\partial \mathbf{v}}{\partial t} + (\nabla \mathbf{v}) \mathbf{v} + \nabla \frac{p}{\rho_*} - \text{div}\left(2\nu_* \mathbf{D}(\mathbf{v})\right) = 0 \tag{4}$$
$$\mathbf{T} = -p\mathbf{I} + 2\mu_* \mathbf{D},$$

where $\mathbf{T}$ is the Cauchy stress tensor, $p = -\frac{1}{3}(\text{tr } \mathbf{T})$ is the mean normal stress that is usually referred to as the mechanical pressure, $\mathbf{v}$ is the velocity of the fluid, $\mathbf{D} = \frac{1}{2}\left(\nabla \mathbf{v} + \left(\nabla \mathbf{v}\right)^T\right)$, μ_* denotes the constant dynamic viscosity and $\nu_* = \frac{\mu_*}{\rho_*}$ is the kinematic viscosity. We will use the subscript $*$ for constants. The list of constants and their values used in this study are shown in Tab. 1.

In the case of a fluid characterized by the Navier-Stokes constitutive relation, the dissipation *Edis* is given by

$$Edis = \mathbf{T} \cdot \mathbf{D}, \tag{5}$$

7

symbol	name	value
ρ_*	density	$1.0\ \frac{kg}{m^3}$
μ_*	dynamic viscosity	$3.71.10^{-3}\ \frac{kg}{s\,m}$
ν_*	kinematic viscosity	$3.71.10^{-3}\ \frac{m^2}{s}$

Table 1: Constant parameters used in calculation.

which in virtue of incompressibility and form of the stress relation (see eq. $(4)_3$) simplifies to

$$Edis = 2\mu_* \mathbf{D} \cdot \mathbf{D}. \tag{6}$$

In principle, since we know the velocity field pointwise due to experimental measurements, we can determine the rate of dissipation given by (6). Instead of trying to crudely estimate the loss of pressure as a consequence of dissipation, we demonstrated in Part 1 of this study (see Švihlová et al. (2016)) how to directly obtain the pressure field once the velocity field is known. That velocity field is supposed to be measured, at least at some subset of points in the flow domain. Consequently, we focused on considering limited amount of points where the measurement of the velocity field could take place, and considering the deviations between the (possibly measured) velocity field and the real velocity field. The real velocity field was in this case also approximated by solution of the Navier-Stokes equations. In the case to be studied here, i.e. flows in aortic valve stenosis, the minimum focus of the known velocity field is the left ventricular outflow tract, which is proximal to the valve.

In this portion of our study, we focus on computations of the pressure drop, kinetic energy and dissipation within/across the geometry representing the stenotic aortic valve. We depict the computed velocity field in the region of the stenosis and distal to it, where secondary flows and recirculation occur. The pressure drop, kinetic energy and dissipation will be shown in geometries representing aortic valve with symmetric stenosis of severity 50%, 60%, 70% and 80% where severity is given as (7). The geometry is limited by the assumption that aortic walls are non-deformable, but with reasonable approximations of the real geometry. The formulation of the boundary conditions used in the model with physiologically relevant pressure and flow profiles follows. Finally, in Sec. 3, we will discuss the results achieved from three-dimensional computations where Navier-Stokes equations are used.

Geometry

The geometry description and the location on the z axis are shown in the Fig. 4, the geometry dimensions are shown in the Fig. 5.

The computational meshes are shown in Fig. 5 and Fig. 6. Firstly, there is a healthy aortic valve and then aortic valves with symmetric severity up to 80%. The severity is given as a relation between the area of the healthy part, approximated here by a circle with radius R, and the area of the stenotic part, approximated by a circle with radius r, i.e.,
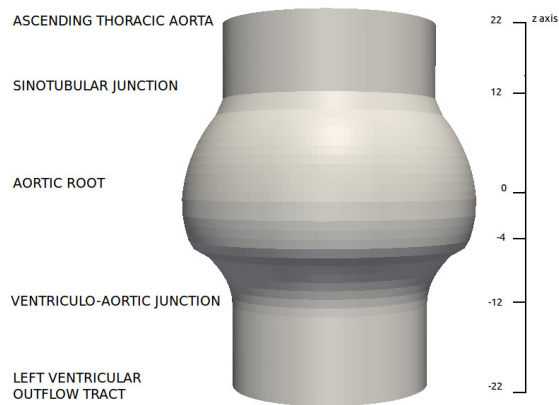
$$severity = (1 - \frac{area_r}{area_R}) \cdot 100\%. \tag{7}$$

Figure 4: **The description of the geometry.** The aortic root is situated between z= -12 and z=12, where z=-12 corresponds to the ventriculo-aortic junction and z=12 to the sinotubular junction. z=0 corresponds to a widest place of aortic root. The part from z=-22 to z=-12 is supposed to be 1cm part of the left ventricular outflow tract, the part between z=12 and z=22 is 1cm part of ascending thoracic aorta.
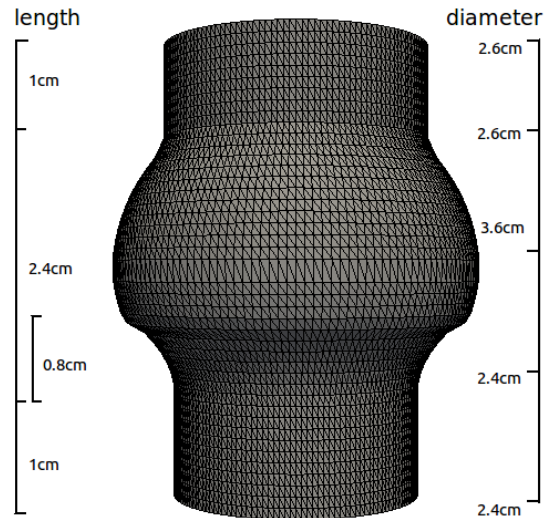

Figure 5: **The geometry dimensions.** Left ventricular outflow tract, aortic root and proximal ascending thoracic aortic dimensions for the healthy case with a rigid wall assumption: The length of the aortic root is 2.4cm here, the part of the aortic root which should be affected by the stenosis is set to 0.8cm. The length of the part representing left ventricle junction is 1cm, the length of the cylinder representing the part of the ascending aorta is 1cm. The diameter of the sinotubular junction is 2.6cm, the diameter of the ventriculo-aortic junction 2.4cm. Finally the maximal diameter of the geometry is 3.6cm.
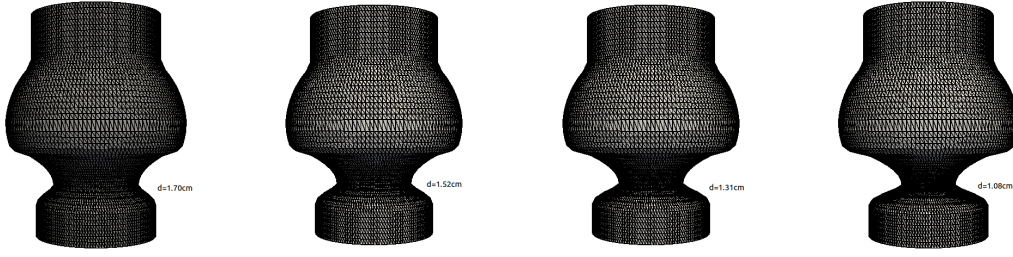
Figure 6: **Geometry representing the stenotic valve with a different severity.** Severity is assumed to be equal $1 - \frac{\pi d^2}{\pi D^2}$, where $D = 2.4$cm is the original diameter of the valve without stenosis and d represents the diameter of the narrowed geometry. For 50% stenosis diameter d=1.70cm, for 60% stenosis d=1.52cm, for 70% stenosis d=1.31cm and finally d=1.07cm for 80% stenosis.

Boundary conditions

In a given domain $\Omega \subset \mathbf{R}^3$, representing the simplified aortic valve, the velocity $\mathbf{v}$ and pressure p satisfy (4). Let us consider the boundary of the domain $\partial\Omega$, which consists of three parts; see Fig. 3. Γ_{wall} denotes the walls and Γ_{in}, Γ_{out} are the inlet and outlet, respectively. In order to be physiologically and clinically relevant, first we consider the known pressure distal to the aortic valve, in the proximal ascending thoracic aorta, (as a Neumann boundary condition on the outlet) and known velocity of blood ejected by, and flowing out of, the left ventricle (as a Dirichlet boundary condition on the inlet). On rigid walls, we consider the no-slip boundary conditions. Hence,

$$
\begin{aligned}
\mathbf{v} &= \mathbf{0} && \text{on } \Gamma_{wall}, \\
\mathbf{v} &= \mathbf{v}_{in} && \text{on } \Gamma_{in}, \\
\mathbf{Tn} - \frac{1}{2}\rho_*(\mathbf{v}\cdot\mathbf{n})_-\mathbf{v} &= -\overline{P(t)}\mathbf{n} && \text{on } \Gamma_{out}.
\end{aligned}
\tag{8}
$$

Here, $\mathbf{n}$ represents the unit normal vector to the boundary and $(\mathbf{v}\cdot\mathbf{n})_-$ denotes the negative part of the function $\mathbf{v}\cdot\mathbf{n}$, as was analyzed in (Bertoglio and Caiazzo, 2016). The value for the constant parameters are given in Tab. 1.

The velocity $\mathbf{v}_{in}$ is given as a parabolic profile with its magnitude scaled by a time dependent factor, $\overline{V(t)}$, representing the mean velocity at the inlet. The velocity time dependent factor $\overline{V(t)}$ is a curve unique for an individual patient. Here, we used the curve displayed in Fig. 7, in which each cardiac cycle is 1s and the systolic ejection period SEP with length $0.3s$ is the time during which the aortic valve is considered open; see Fig. 8. During the SEP, the velocity initially is $0m/s$ (no flow), increases to v_{max}, and then decreases to $0m/s$ (at which part the SEP ends). For the purpose of this work, we used $v_{max} = 0.7m/s$ for all geometries.
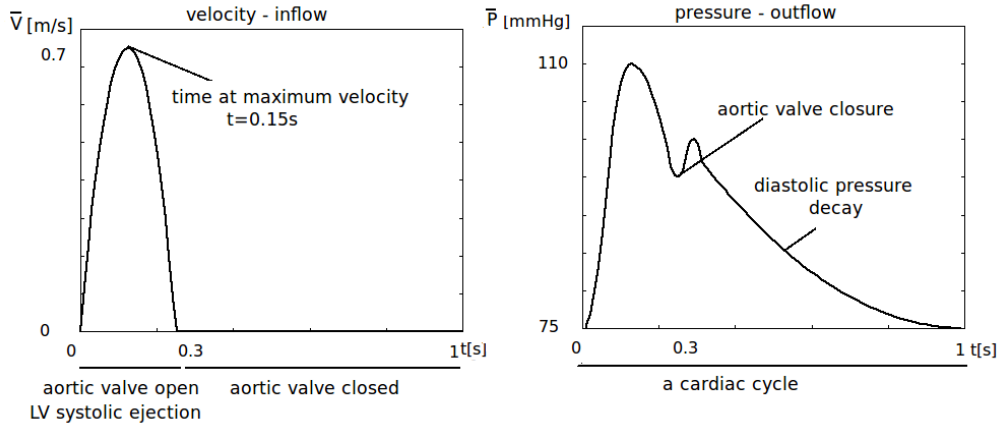
Figure 7: The prescribed outlet pressure and inlet velocity functions $\overline{P(t)}$ and $\overline{V(t)}$ as functions of time.

Note that the mean velocity $\mathbf{v}_{mean} = \frac{2}{3}\mathbf{v}_{max} = 0.45$m/s, the systolic ejection period $SEP = 0.3s$, time for maximum velocity is at 0.15s, and the area of input cross-section $A_{valve} = \pi\frac{D^2}{4} = 4.5cm^2$. The diameter of the input plane is $D = 2.4cm$. The corresponding stroke volume SV (volume of the blood ejected by the left ventricle per heart beat) can then be computed from the left ventricular ejection volumetric flow rate F as

$$SV = \int_{t=0}^{1} F\,dt = \int_{t=0}^{1} A_{valve} * \overline{V(t)}\,dt = A_{valve} * SEP * \mathbf{v}_{mean} \doteq 61ml. \tag{9}$$
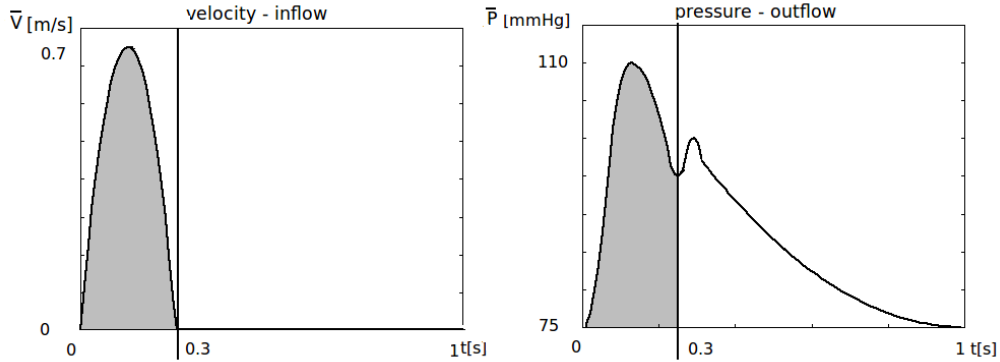
Figure 8: Systolic ejection period SEP.

At the outlet, i.e., the proximal ascending thoracic aorta, we prescribe the pressure mean value $\overline{P(t)}$, which is based on information from measurements in the aorta as a function of time. At the output, recirculation may occur, and can lead to instabilities. We assume that no aortic valve regurgitation is present, and use backflow stabilization used at the outlet as developed in Bertoglio and Caiazzo (2016) and Braack and Mucha (2014).

The function $\overline{P(t)}$ can depend on the stenosis severity. As aortic valve stenosis progresses, if and when left ventricular intrinsic systolic function (contractility) decompensates and cannot maintain (i.e., contractility is not high enough) adequate stroke volume in the face of elevated afterload posed by the stenotic valve, systemic arterial hypotension may occur. This occurs, but is uncommon. We have assumed

11

adequate (which must actually be supranormal) left ventricular contractility to maintain stroke volume and distal aortic pressure. Thus, for the purposes of this work, we used the function $\overline{P(t)}$, see Fig. 8 (right), such that the peak systolic aortic pressure p_{max} = 110mmHg and the nadir diastolic aortic pressure p_{min} = 75mmHg. For better illustration, we use units of millimeters Hg for pressure (1 Pa = 0,0075 mmHg).

3. Calculation of the pressure drop and energy dissipation across a stenotic aortic valve

FEniCS software for solving partial differential equations Logg et al. (2012) was used to compute the problem eq.(4)&(8) by the finite element method. The time derivatives in the equations were approximated by the Crank-Nicholson scheme. Time interval of systolic ejection period length 0.3s was computed, and an adaptive time step was used. The time step length varies from 1E-2 to 2E-3 for mild stenotic cases with 50% and 60% severity. Because of high velocities in the narrowed part, the length of time step had to be finer in more severe cases. The time step length varies from 1E-3 to 2E-4 for 70% case and from 1E-3 to 5E-5 for 80% .

In this section, we plot the pressure p_Γ introduced in (10), dissipation $Edis_\Gamma$ specified in (11) and kinetic energy Ek_Γ defined as (12) along the centerline for meshes with different severities, see (7), namely 50%, 60%, 70% and 80%. The centerline is an axis passing through the vessel; Γ denotes cross-sectional area along the centerline, see Fig. 9.

$$p_\Gamma = \frac{\int_\Gamma p\, dS}{\text{area}(\Gamma)} \tag{10}$$

$$Edis_\Gamma = \frac{2\mu_* \int_\Gamma \mathbf{D}:\mathbf{D}\, dS}{\text{area}(\Gamma)} \tag{11}$$

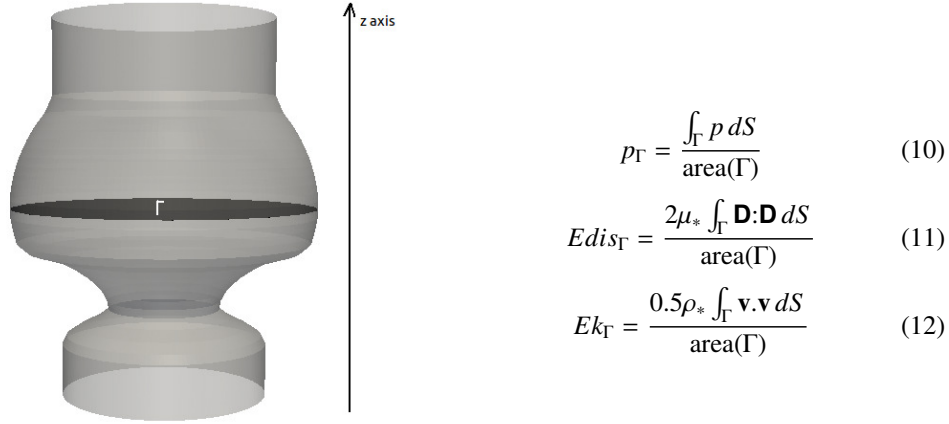$$Ek_\Gamma = \frac{0.5\rho_* \int_\Gamma \mathbf{v}.\mathbf{v}\, dS}{\text{area}(\Gamma)} \tag{12}$$

Figure 9: Cross-section areas Γ along the centerline, which corresponds to the z axis.

Graphs of pressure, kinetic energy and energy dissipation, at time at maximum velocity, but varying as functions of position, are shown in Fig. 11. Similar graphs of time averaged values over the systolic ejection period, but again varying as functions of position, are displayed in Fig. 12.

Time averaged value of pressure is calculated over the SEP as

$$p_{\Gamma aver} = \int_0^{0.3} p_\Gamma\, dt. \tag{13}$$

Kinetic energy and energy dissipation are calculated similarly.

Figure 10 depicts transvalvular pressure drop as a function of time over a range of stenosis severities. Tables 2 and 3 display maximum and mean SEP transvalvular pressure drops over the range of stenosis severities. These data are consistent with measured data in Garcia et al. (2006). Classically, stenoses are

thought to cause adverse hemodynamic and other sequelal once stenosis severity is in the range of 70-80%. Our findings are consistent with this clinical experience.

Figures 11 and 12 show the variables averaged over cross-sectional area Γ as functions of the z coordinate (see Fig. 9), at time t=0.15s, and averaged over the SEP, respectively. Graphs of the time evolution of variables (i.e., as time-varying functions) during the SEP at specified z coordinates are shown in Fig. 13-17.

The computations here are limited by the fact that stenosis here is symmetric. The study of symmetric versus asymmetric stenoses in simplified cylindrical geometries is provided in Appendix. The pressure drop and energy dissipation are higher in geometries with asymmetric obstruction than in the symmetric problems. The computed results shown in Appendix are in good agreement with this statement.
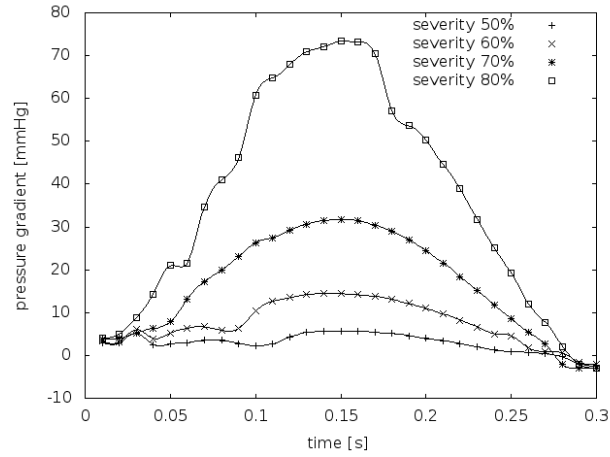
Figure 10: Pressure drop across the aortic valve during the SEP, for different degrees of of stenosis. Pressure drop is defined as a difference between the pressure averaged over cross-sectional area of output and pressure averaged over cross-sectional area of input, i.e. the difference between p_Γ at z=-22 and p_Γ at z=22.

sev	input pressure	pressure drop
50	115.6	5.6
60	124.3	14.3
70	141.7	31.7
80	183.3	73.3

sev	input pressure	pressure drop
50	101.6	3.0
60	106.1	7.5
70	115.1	16.5
80	135.0	36.4

Table 2: Computed input integral pressure (i.e. averaged over the input cross-sectional area) and the pressure drop at time at maximum velocity. Output integral pressure was fixed (prescribed as a boundary condition) to 110mmHg.

Table 3: Computed input integral pressure (i.e. averaged over the input cross-sectional area) and the pressure drop as an average value over the SEP. Output integral pressure was fixed (prescribed as a boundary condition) to 98.6mmHg.
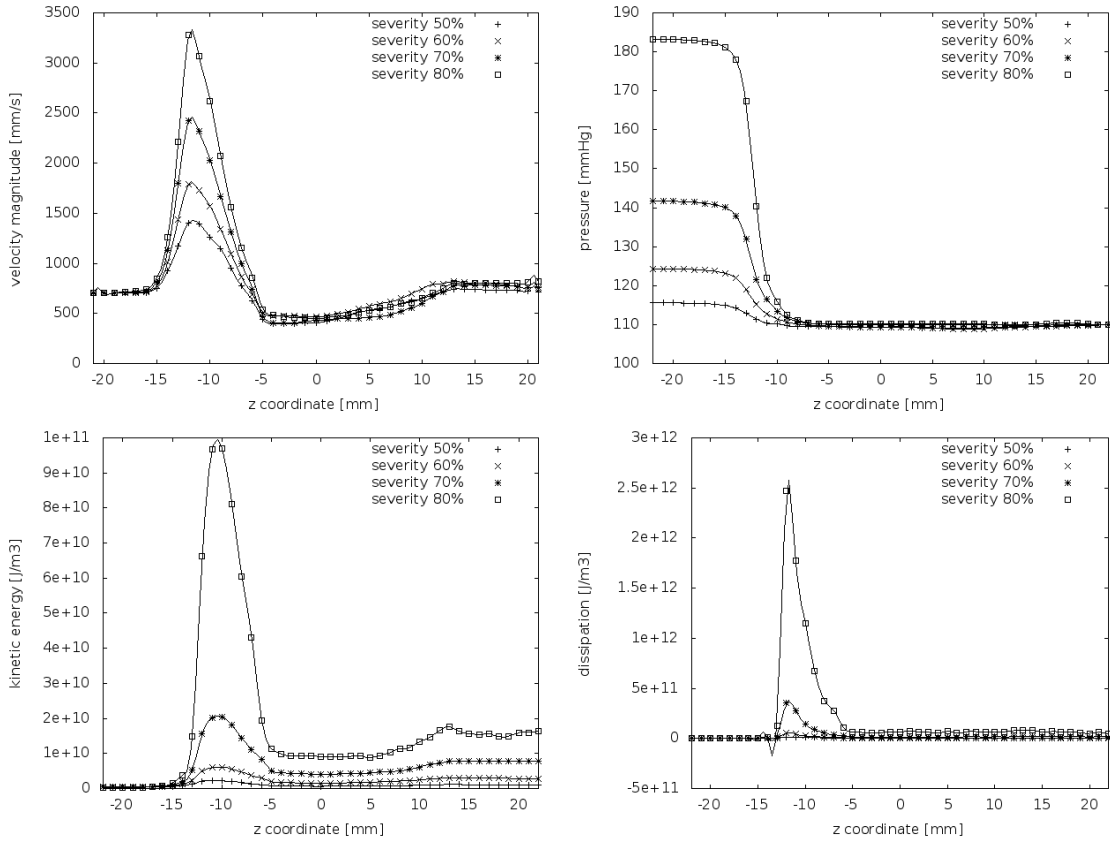
Figure 11: Velocity, pressure, kinetic energy and energy dissipation averaged over cross-sectional area Γ, varying as functions of the z coordinate (length), set at the time of maximum velocity ($t = 0.15$s)

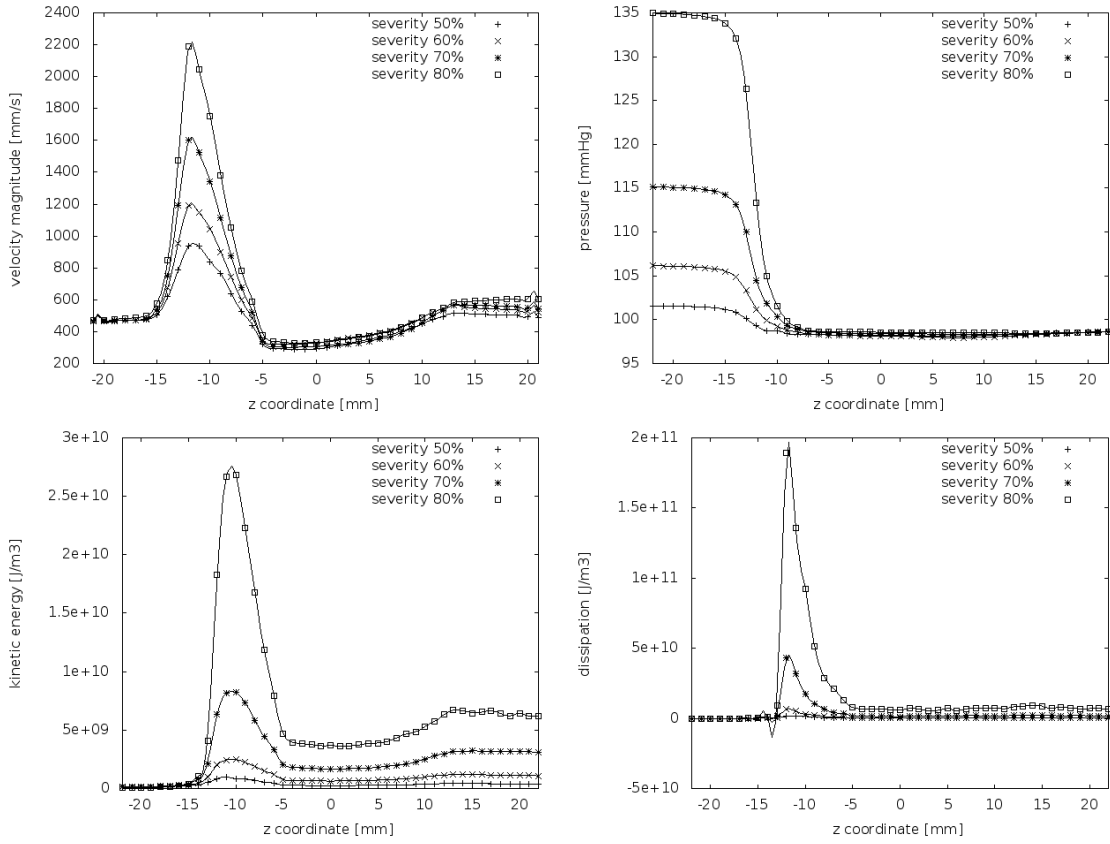Figure 12: Velocity, pressure, kinetic energy and energy dissipation averaged over space (cross-sectional area Γ) and time (SEP), varying as functions of the z coordinate (length).
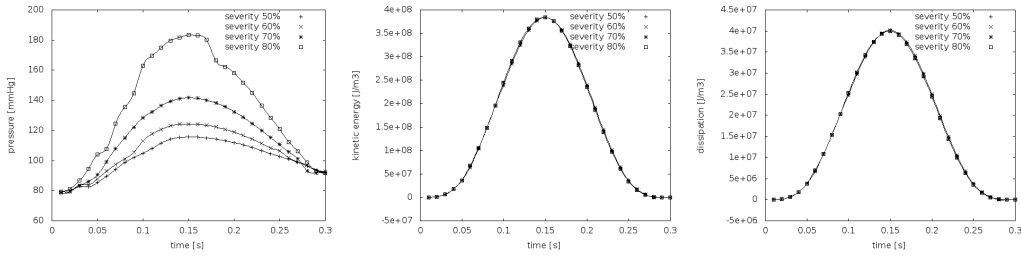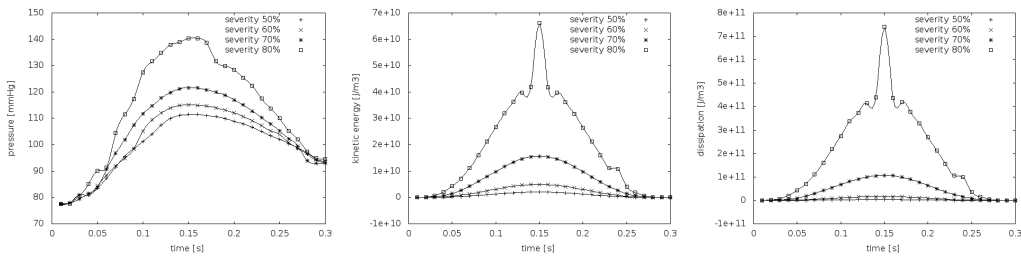
Figure 13: Pressure, kinetic energy and energy dissipation averaged over cross sectional area Γ, varying as functions of time; at z=-22.
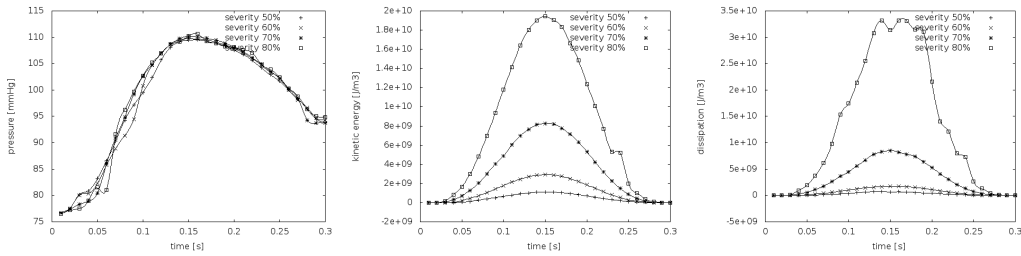

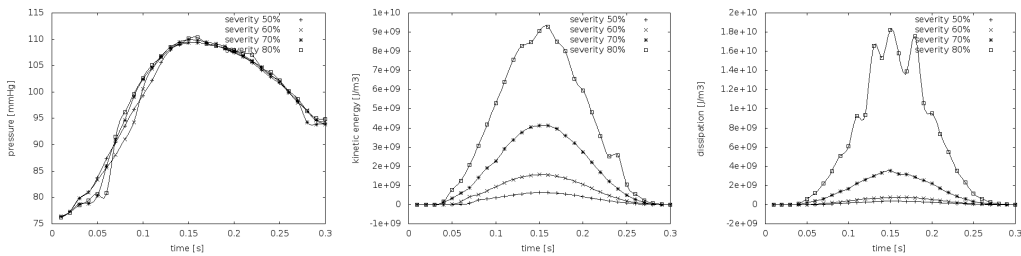
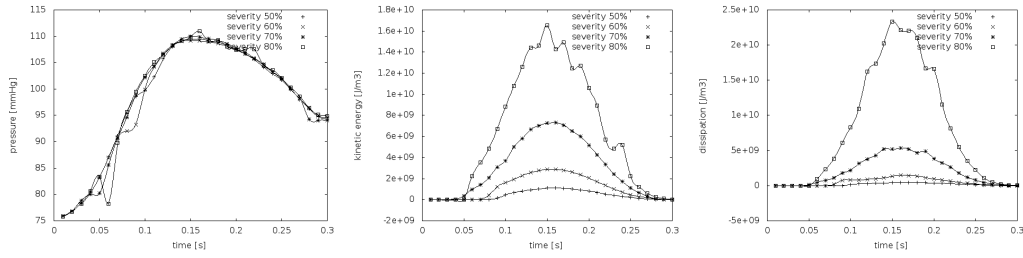Figure 14: Pressure, kinetic energy and energy dissipation averaged over cross sectional area Γ, varying as functions of time; at z=-12.

Figure 15: Pressure, kinetic energy and energy dissipation averaged over cross sectional area Γ, varying as functions of time; at z=-6.

Figure 16: Pressure, kinetic energy and energy dissipation averaged over cross sectional area Γ, varying as functions of time; at z=0.

Figure 17: Pressure, kinetic energy and energy dissipation averaged over cross sectional area Γ, varying as functions of time; at z=12.

4. Discussion

In the previous study, we developed a state-of-art rigorous mathematical approach, incorporating physiologically relevant conditions, to modeling blood flow across cardiovascular stenoses. This approach can be applied to studying intra-cardiac and intra-arterial flows. In this manuscript, we have applied our model to a complex pathophysiological state - native aortic valve stenosis. Although we have modeled this in the absence of coexistent aortic valve regurgitation, our approach can be applied to the mixed disease state. Most importantly, the model can as extract a wide range of output data from limited input data - with *ab initio* specification of the inflow velocity profile and the outflow pressure profile. This enhances its potential clinically relevancy.

With respect to limitations, there are two oversimplifications. The first oversimplification is principally geometric, and is the specification of valve structure and stenosis in the absence of actual valve leaflets, with stenosis modeled as a reduction in housing/wall diameter. The absence of valve leaflets necessitates up-front specification of the absence of regurgitation via a backstop. However, our upcoming studies are incorporating moving actual valve leaflets, and modeling stenosis as a reduction in leaflet motion and systolic (for the aortic valve) ejection orifice expansion and subsequent contraction. Nonetheless, the current model can yet be applied to arterial blood flow in its current form. The second limitation is that a rigid aorta is assumed. Many previous studies have incorporated aortic wall mechanics, but using simplified lumped parameter approaches. Further work will address this oversimplification as well.

The existing body of literature and extant work on modeling of cardiovascular blood flow generally is limited by important oversimplifications and frank conceptual errors - both mathematical and mechanical. A need for rigorous mathematical/mechanical modeling of cardiac and vascular function and blood flow thus is required. This work is a substantial shift in modeling approaches to cardiovascular system function from which further progress may be made.

Acknowledgments

Akins, C. W., Travis, B., and Yoganathan, A. P. (2008). Energy loss for evaluating heart valve performance. *The Journal of Thoracic and Cardiovascular Surgery*, 136(4):820–833.

Alexandrov, A. V., Bladin, C. F., Maggisano, R., and Norris, J. W. (1993). Measuring carotid stenosis. Time for a reappraisal. *Stroke*, 24(9):1292–1296.

Attinger, E., Anné, A., and McDonald, D. (1966). Use of Fourier Series for the Analysis of Biological Systems. *Biophysical Journal*, 6(3):291–304.

Berger, M., Berdoff, R. L., Gallerstein, P. E., and Goldberg, E. (1984). Evaluation of aortic stenosis by continuous wave Doppler ultrasound. *Journal of the American College of Cardiology*, 3(1):150–156.

Bertoglio, C. and Caiazzo, A. (2016). A Stokes-residual backflow stabilization method applied to physiological flows. *Journal of Computational Physics*, 313:260–278.

Bhattacharyya, S., Khattar, R., Chahal, N., Moat, N., and Senior, R. (2013). Dynamic assessment of stenotic valvular heart disease by stress echocardiography. *Circulation: Cardiovascular Imaging*, 6(4):583–589.

Braack, M. and Mucha, P. B. (2014). Directional Do-Nothing Condition for the Navier-Stokes Equations. *Journal of Computational Mathematics*, 32(5):507–521.

Carroll, J. D. (1993). Cardiac catheterization and other imaging modalities in the evaluation of valvular heart disease. *Current opinion in cardiology*, 8(2):211–215.

Dasi, L. P., Simon, H. A., Sucosky, P., and Yoganathan, A. P. (2009). Fluid mechanics of artificial heart valves. *Clinical and Experimental Pharmacology and Physiology*, 36(2):225–237.

Eckstein, R. W., Liebow, I. M., and Wiggers, C. J. (1946). Limb blood flow and vascular resistance changes in dogs during hemorrhagic hypotension and shock. *The American journal of physiology*, 147(4):685–694.

Fischer, J. L., Haberer, T., Dickson, D., and Henselmann, L. (1995). Comparison of Doppler echocardiographic methods with heart catheterisation in assessing aortic valve area in 100 patients with aortic stenosis. *Heart*, 73(3):293–298.

Ford, L. E., Feldman, T., Chiu, Y. C., and Carroll, J. D. (1990). Hemodynamic resistance as a measure of functional impairment in aortic valvular stenosis. *Circulation Research*, 66(1):1–7.

Garcia, D., Kadem, L., Savéry, D., Pibarot, P., and Durand, L. (2006). Analytical modeling of the instantaneous maximal transvalvular pressure gradient in aortic stenosis. *Journal of Biomechanics*, 39(16):3036–3044.

Go, A. S., Mozaffarian, D., Roger, V. L., Benjamin, E. J., Berry, J. D., Blaha, M. J., Dai, S., Ford, E. S., Fox, C. S., Franco, S., Fullerton, H. J., Gillespie, C., Hailpern, S. M., Heit, J. A., Howard, V. J., Huffman, M. D., Judd, S. E., Kissela, B. M., Kittner, S. J., Lackland, D. T., Lichtman, J. H., Lisabeth, L. D., Mackey, R. H., Magid, D. J., Marcus, G. M., Marelli, A., Matchar, D. B., McGuire, D. K., Mohler, E. R., Moy, C. S., Mussolino, M. E., Neumar, R. W., Nichol, G., Pandey, D. K., Paynter, N. P., Reeves, M. J., Sorlie, P. D., Stein, J., Towfighi, A., Turan, T. N., Virani, S. S., Wong, N. D., Woo, D., and Turner, M. B. (2013). Heart disease and stroke statistics–2014 update: a report from the American Heart Association. *Circulation*, 129(3):e28–e292.

Gorlin, R. and Gorlin, S. (1951). Hydraulic formula for calculation of the area of the stenotic mitral valve, other cardiac valves, and central circulatory shunts. i. *American Heart Journal*, 41(1):1–29.

Hakki, A. H., Iskandrian, A. S., Bemis, C. E., Kimbiris, D., Mintz, G. S., Segal, B. L., and Brice, C. (1981). A simplified valve formula for the calculation of stenotic cardiac valve areas. *Circulation*, 63(5):1050–1055.

Hatle, L., Angelsen, B. A., and Tromsdal, A. (1980). Non-invasive assessment of aortic stenosis by Doppler ultrasound. *Heart*, 43(3):284–292.

Hatle, L., Brubakk, A., Tromsdal, A., and Angelsen, B. (1978). Noninvasive assessment of pressure drop in mitral stenosis by Doppler ultrasound. *Heart*, 40(2):131–140.

Kosturakis, D., Goldberg, S. J., Allen, H. D., and Loeber, C. (1984). Doppler echocardiographic prediction of pulmonary arterial hypertension in congenital heart disease. *The American Journal of Cardiology*, 53(8):1110–1115.

Leggett, M. and Otto, C. M. (1996). Aortic valve disease. *Current opinion in cardiology*, 11(2):120–125.

Logg, A., Mardal, K., and Wells, G. (2012). *Automated Solution of Differential Equations by the Finite Element Method*. Springer Berlin Heidelberg.

Rodriguez, G., Arnaldi, D., Campus, C., Mazzei, D., Ferrara, M., Picco, A., Famà, F., Colombo, B. M., and Nobili, F. (2011). Correlation between Doppler Velocities and Duplex Ultrasound Carotid Cross-sectional Percent Stenosis. *Academic Radiology*, 18(12):1485–1491.

Schwartz, L. B., Purut, C. M., Craig, D. M., Smith, P. K., Moawad, J., and McCann, R. L. (1997). Measurement of Vascular Input Impedance in Infrainguinal Vein Grafts. *Annals of Vascular Surgery*, 11(1):35–43.

Schwartz, L. B., Purut, C. M., O'Donohoe, M. K., Smith, P. K., Hagen, P., and McCann, R. L. (1991). Quantitation of vascular outflow by measurement of impedance. *Journal of Vascular Surgery*, 14(3):353–363.

Spencer, M. P. and Edmunds, L. H. (1968). Evaluation of Operative Left Ventricular Outflow Tract Lesions with a Fluid Impedance Plot. *Circulation*, 37(6):912–921.

Švihlová, H., Hron, J., Málek, J., Rajagopal, K., and Rajagopal, K. (2016). Determination of pressure data from velocity data with a view toward its application in cardiovascular mechanics. Part 1. Theoretical considerations. *International Journal of Engineering Science*, 105:108–127.

Warth, D. C., Stewart, W. J., Block, P. C., and Weyman, A. E. (1984). A new method to calculate aortic valve area without left heart catheterization. *Circulation*, 70(6):978–983.

APPENDIX

Studies of symmetric versus asymmetric stenoses

We computed the pressure, kinetic energy, and energy dissipation, in simplified cylindrical geometries, as opposed to more clinically relevant geometry. Meshes representing stenoses of up to 80% severity are shown in Fig. 18 and Fig. 19 for symmetric stenosis and for the axial asymmetric stenosis, respectively. The computed quantities: pressure, kinetic energy, and energy dissipation, are shown at the peak systolic ejection time (t=0.15s) in Fig. 20 and Fig. 21.
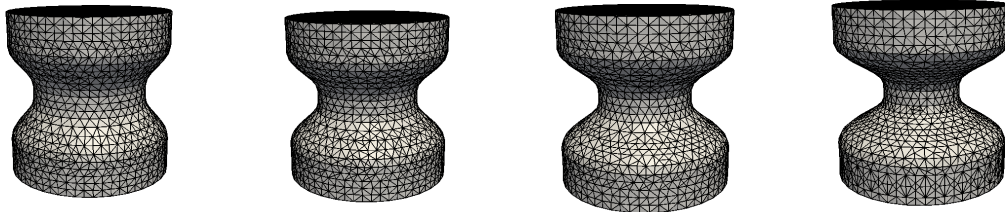
Figure 18: Three-dimensional computational meshes representing symmetric stenoses of 50%, 60%, 70% and 80% severities.
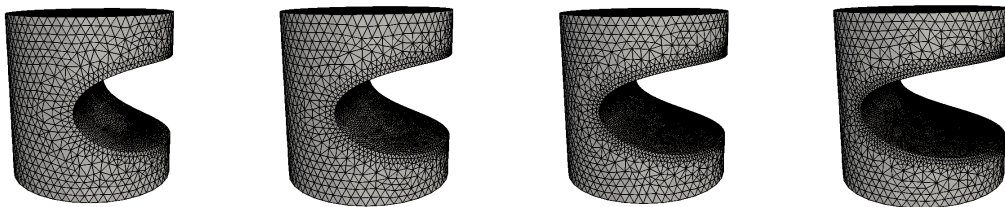

Figure 19: Three-dimensional computational meshes representing asymmetric stenoses of 50%, 60%, 70% and 80% severities.
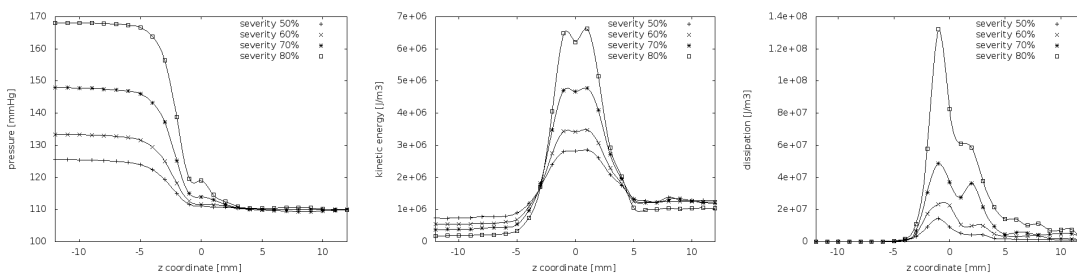

Figure 20: Trans-stenosis pressure drop, kinetic energy and dissipation over cross-sections as a function of the position along the centerline for different symmetric geometries, at the time of peak systolic ejection velocity. Peak velocity here was set to 1m/s.
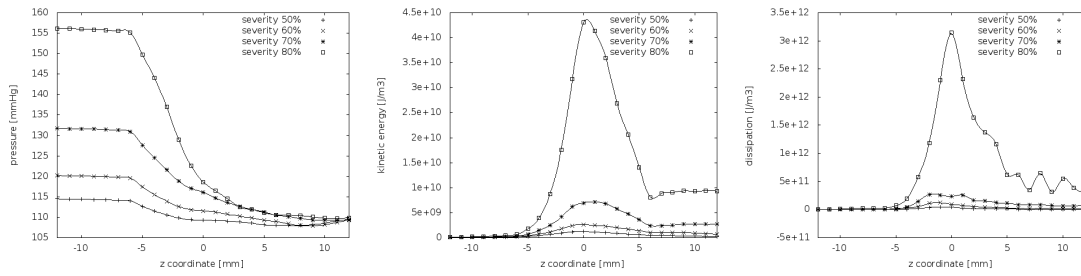
Figure 21: Trans-stenosis pressure drop, kinetic energy and dissipation over cross-sections as a function of the position along the centerline for different asymmetric geometries, at the time of peak systolic ejection velocity. Peak velocity here was set to 0.7m/s for 50%, 60% and 70% case but for 80% case it was decreased to 0.6m/s.